45th AIAA Aerospace Sciences Meeting and Exhibit
8 - 11 January 2007, Reno, Nevada

AIAA 2007-1316

The effect of crossflow on vortex rings

Rajes Sau* and Krishnan Mahesh†
University of Minnesota, Minneapolis, MN, 55414, USA

DNS is performed to study passive scalar mixing in vortex rings in the presence, and absence of crossflow. For vortex rings without crossflow, the 'formation number' (Gharib *et. al* 1998) is found to be 3.6. Simulations are performed for a range of stroke ratios encompassing the formation number. In the absence of crossflow, the optimal stroke ratio for mixing and entrainment is shown to be at the formation number; the trailing column is not seen to be as beneficial as the ring itself. However, in the presence of crossflow, the trailing column is shown to contribute significantly to the overall mixing and entrainment. The trailing column enhances the entrainment significantly because of the high pressure gradient created by deformation of the column upon interacting with crossflow. It is shown that the crossflow reduces the stroke ratio beyond which the trailing column forms. This reduction in stroke ratio is due to entrainment of crossflow fluid during formation of the ring, and depends on the velocity ratio.

I. Introduction

Jets in cross-flow are central to a variety of important applications such as dilution holes in combustors, fuel injectors, pollutant dispersion from smoke stacks, thrust vectoring of turbojets, and V/STOL aircraft. There is considerable incentive to develop the ability to actively control jets in crossflow. This paper is motivated by the experimental observations on the use of pulsing to control the mixing characteristics of jets in crossflow (e.g. Eroglu *et al* 2001, M'Closkey *et al.* 2002, Blossey *et al.* 2001, Karagozian *et al.* 2003). Experiments show that pulsation of the jet results in the formation of vortex rings, whose strength and spacing are dictated by the frequency and duty cycle of the jet for a given jet and crossflow combination (Eroglu *et al.* 2001). The resulting flow appears to improve mixing rate and increase the entrainment. This paper therefore examines the basic problem of how a vortex ring mixes with stationary and crossflow fluid. The experimental results (Shapiro *et al.* 2003, M'Closkey *et al.* 2002) relate the optimal pulse width for maximum penetration of vortical structures to the universal time scale of vortex ring formation, namely 'formation number' (Gharib *et al.* 1998). Johari (2005) presents scaling arguments, based on the motion of individual vortex rings in stationary fluid, for the penetration and mixing of pulsed jets in crossflow. Classification schemes are developed using the formation number and the stroke ratio obtained from the frequency and duty cycle of the pulsed jet, thus completely ignoring the effect of crossflow on individual vortex rings.

The objective of the present investigation is to study the effect of crossflow on vortex ring dynamics, mixing and entrainment characteristics, using DNS. The effect of stroke ratio on entrainment by vortex rings are also studied. This paper is organized as follows. Section II discusses the problem and details of the simulations. Simulation results are presented in Section III. The section III A discusses the formation number, mixing and entrainment characteristics for vortex rings in the absence of crossflow. The section III

*Graduate Research Assistant
†Associate Professor

Copyright © 2007 by the American Institute of Aeronautics and Astronautics, Inc. All rights reserved.

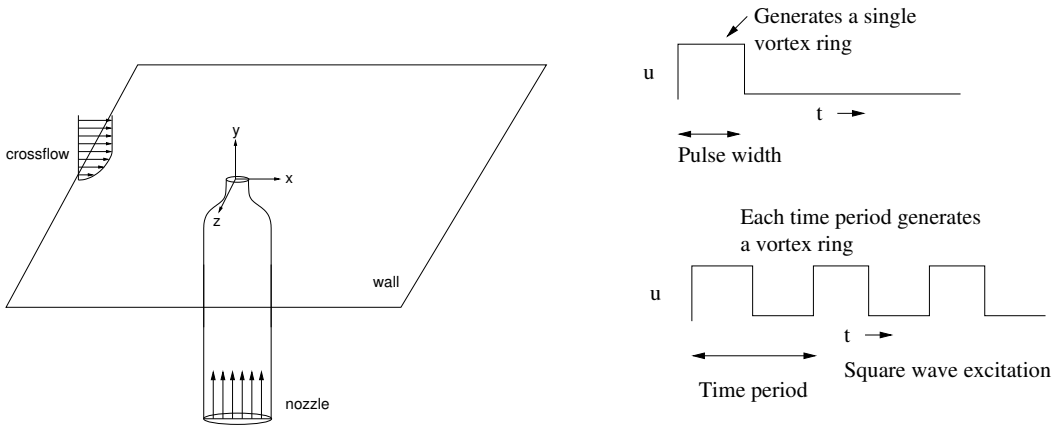

Figure 1. A Schematic of the problem along with the time history of the inflow velocity boundary condition to generate the vortex ring.

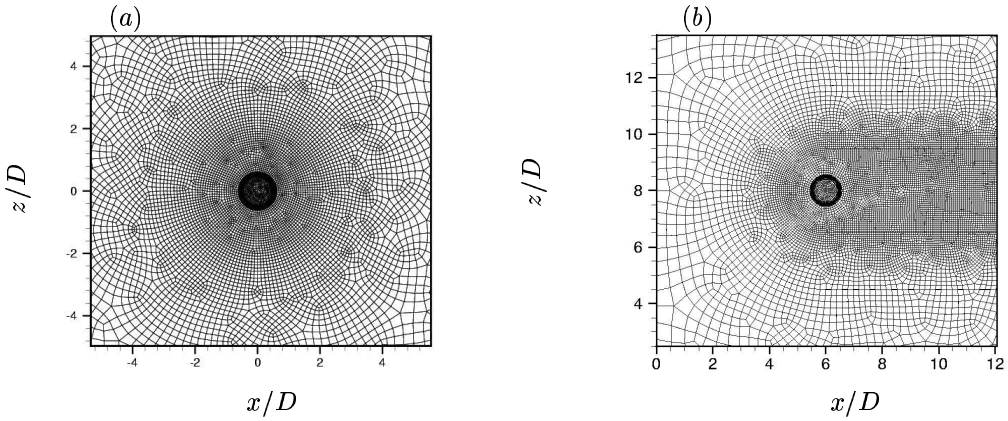

Figure 2. Horizontal slice of the meshes used for (a) vortex ring without crossflow (b) Vortex ring in crossflow.

B presents the results for vortex rings in the presence of crossflow. The vortex ring dynamics in crossflow is shown in section III B-1. The mixing and entrainment characteristics of vortex rings in the presence of crossflow are examined in section III B-2. Concluding remarks are presented in section IV.

II. Simulation details

A. Problem Statement

Figure 1 shows a schematic of the problem. The origin is at the center of the nozzle exit. The nozzle exit plane and the wall are located in the plane $y = 0$. The axis of symmetry of the cylindrical nozzle (3 : 1 diameter ratio) is along the y axis. The crossflow is in the x direction. The crossflow velocity varies along the direction perpendicular to the wall. u_∞ is the crossflow free–stream velocity. Simulations are performed with and without the crossflow.

In experiments, vortex rings are generated by the motion of a piston pushing a column of fluid of length L through an orifice or nozzle of diameter D. This results in the separation of boundary layer at the edge

of the orifice or nozzle and its subsequent spiral roll-up. In simulations, pushing of a column of fluid by the piston is modeled by specifying a uniform velocity (time dependent) at the entrance of the nozzle (Rosenfeld *et al.* 1998) as shown in figure 1. Each time period or cycle of the pulsation of the jet leads to a vortex ring. To simulate a single vortex ring, only the first time period of a square wave excitation is supplied at the nozzle inflow. The nozzle inflow plane velocity is set to zero for time greater than the pulse width τ. The stroke length L for pulse width τ through nozzle area A is defined by

$$L = \frac{1}{A}\int_0^\tau \int_A u_{jet}\, dA\, dt.$$

Strouhal number St is defined as $fD/\overline{u}_j$ where D is nozzle exit diameter, f pulsing frequency and $\overline{u}_j$ is the mean jet velocity obtained by averaging u_j over the nozzle cross–section in one time period. Duty cycle α is defined as the percentage of jet-on during each cycle, i.e. the ratio of pulse width to the time period). St and α are the parameters governing the pulsed jet through nozzle. The stroke ratio for a single vortex ring, defined by L/D is directly related to St and α as each cycle generates a vortex ring. For square wave excitation (as shown in figure 1) and top-hat velocity profile at the nozzle inflow plane the relation is as follows

$$\text{Stroke ratio } \frac{L}{D} = \left(\frac{1}{St}\right)\left(\frac{1}{2\alpha}\right).$$

For 50% duty cycle, the stroke ratio is exactly inverse of the Strouhal number.

DNS of single vortex rings are performed for stroke ratios varying from 1.6 to 6 with and without the crossflow. Both the formation and post-formation phases of the vortex ring are studied. Experimental results for vortex rings with stroke ratio 2 and 6 are used to validate our simulation. The effect of crossflow is studied by performing simulation at the velocity ratio r (defined as $\overline{u}_j/u_\infty$) of 3 and 1.5. The Reynolds number of the flow based on the pulse velocity (U_p) at the nozzle entrance and the nozzle exit diameter (D) is 600.

B. Numerical details

The numerical scheme solves the incompressible Navier Stokes equations

$$\frac{\partial u_i}{\partial t} + \frac{\partial u_i u_j}{\partial x_j} = -\frac{\partial p}{\partial x_i} + \nu\frac{\partial^2 u_i}{\partial x_j x_j} \quad , \quad \frac{\partial u_i}{\partial x_i} = 0. \tag{1}$$

on unstructured grids. Here u_i, p and ν denote the velocities, pressure and kinematic viscosity respectively. The density of the fluid is assumed constant and is absorbed into the pressure. The numerical scheme has been described in detail by Mahesh *et al.* (2004). The algorithm stores the Cartesian velocities and the pressure at the centroids of the cells (control volumes) and the face normal velocities are stored independently at the centroids of the faces. The scheme is a predictor–corrector formulation which emphasizes discrete energy conservation on unstructured grids. This property makes the algorithm robust at high Reynolds numbers without numerical dissipation. The predicted velocities at the control volume centroids are obtained using the viscous and the non–linear terms of equation 1 which are then used to predict the face normal velocities on the faces. The predicted face normal velocity is projected so that continuity is discretely satisfied. This yields a Poisson equation for pressure which is solved iteratively using a multigrid approach. The pressure field is used to update the Cartesian control volume velocities. Implicit time–stepping is performed using a Crank–Nicholson scheme. The algorithm has been validated for a variety of problems over a range of Reynolds numbers (Mahesh *et al.* 2004).

The passive scalar is computed by solving the advection-diffusion equation

$$\frac{\partial C}{\partial t} + \frac{\partial C u_j}{\partial x_j} = \frac{\nu}{Sc}\frac{\partial^2 C}{\partial x_j x_j}, \tag{2}$$

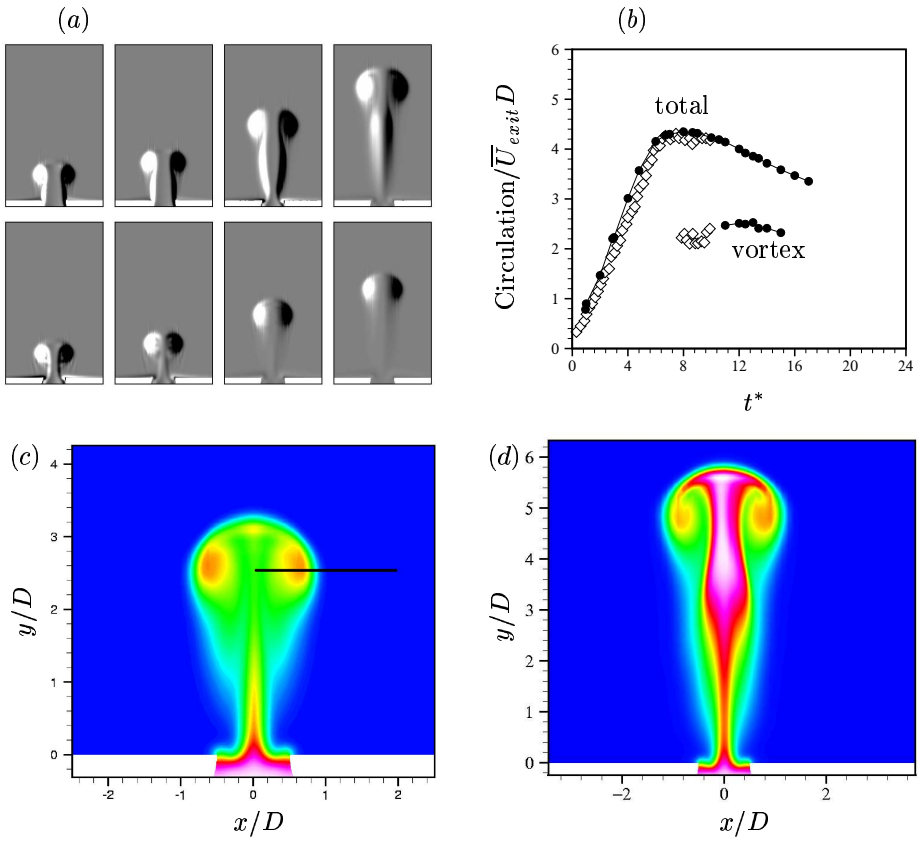

Figure 3. (a) Evolution of vorticity field during formation and post-formation phases of the vortex ring for $L/D = 6$ (top row) and $L/D = 2$ (bottom row). The formation time instants are 3.0, 4.0, 7.0 and 10.0 (from left). Note the vortex ring with a 'trailing column' for the higher stroke ratio. (b) Time evolution of the total and vortex circulation for $L/D = 6$: $\diamond$, experiment (Gharib *et al.*, 1998);$-\circ-$, simulation. Instantaneous contours of passive scalar on $z = 0$ plane for (c) $L/D = 2$ at t^*=6.552, (d) $L/D = 6$ at t^*=10.08. Note the scalar mixing in the core of the vortex ring, downstream scalar deposition as the vortex ring propagates. Scalar profiles along the line shown in figure (c) are studied to compare the scalar mixing inside the ring.

where C is the concentration of the scalar. The fluid emerging from the nozzle-exit has a value of $C = 1.0$, and the ambient fluid has $C = 0.0$. The spatial derivatives are computed using a predictor–corrector method (Muppidi 2006). The scalar field is first advanced using a second–order central difference scheme. The predicted scalar field is corrected in regions of scalar overshoot using a first order upwind scheme. This corrector step ensures that locally, the passive scalar concentration is bounded (*i.e.* $C \in [0, 1]$). The scalar is advanced in time explicitly using second order Adam-Bashforth scheme in an inner loop.

C. Computational domain & boundary conditions

The computational domain above the nozzle exit spans $16D \times 24D \times 16D$ in x, y and z directions for simulations of vortex ring without crossflow. The domain includes the $10D$ length of nozzle upstream of the nozzle exit. The computational mesh is unstructured and hexahedral elements are used. Figure 2(a) shows a horizontal slice of the mesh. Note the very fine elements near the nozzle exit. The boundary conditions are specified as follows. At the nozzle inflow plane, a top–hat velocity profile is specified for a length of time τ. Wall boundary conditions are specified at the nozzle walls, outer walls and wall at the nozzle exit plane. A zero-gradient boundary condition is used at the outflow ($y/D = 24$).

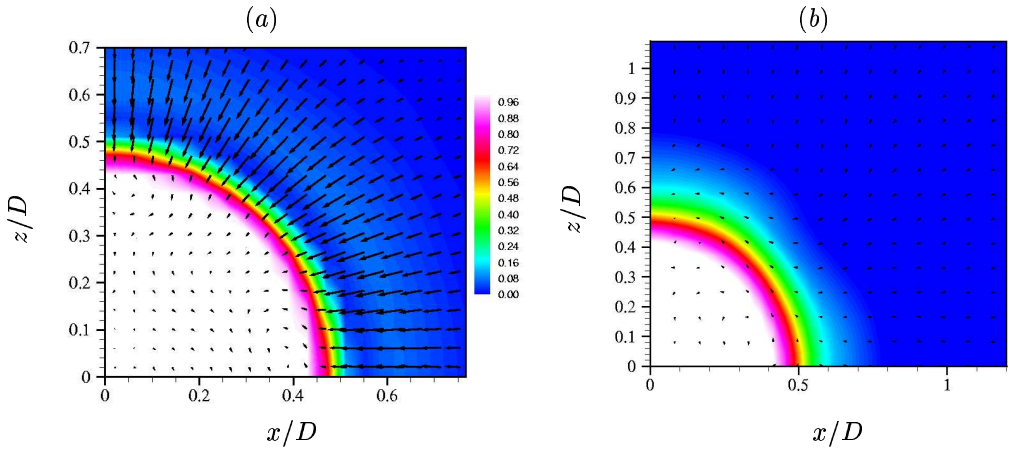

Figure 4. (a) The horizontal cross–section of the emerging shear layer for $L/D = 2$ at $y/D = 0.1$ at $t^* = 1.008$. Contours of scalar along with in–plane velocity vectors. As the problem is axisymmetric, only the first quadrant is shown. Note the length and direction of the velocity vectors in the ambient field. (b) The horizontal cross–section of the trailing jet for $L/D = 6$ at $y/D = 0.6$ at $t^* = 5.04$. Contours of scalar along with in–plane velocity vectors. Note that the in–plane velocity vectors are of zero magnitude.

In the case of crossflow, the computational domain spans $21D \times 20D \times 16D$ above the nozzle exit in x, y and z directions respectively and includes the $10D$ length of nozzle. The computational mesh consist of unstructured hexahedral elements. Figure 2(b) shows the horizontal cross section of the mesh for this case. Very fine mesh elements are used near the nozzle exit and along the direction of the crossflow. The crossflow is simulated as a laminar flow over a flat plate. The velocity field from the analytical solution of the Blasius boundary layer is specified at the inflow plane of the crossflow, $6D$ upstream of the nozzle exit. The velocity field is such that, in the absence of the nozzle fluid, the crossflow has the prescribed $\delta_{50\%}$ at the centre of the nozzle exit. On the spanwise boundaries ($z/D = \pm 8$), the velocity field corresponding to laminar crossflow over flat plate is prescribed. Freestream velocity boundary conditions are specified on the top boundary at $y/D = 20$. The boundary conditions at the exit plane ($x/D = 21$) and at the nozzle inflow plane, are same as in the case of simulations without crossflow.

III. Results

A. Vortex ring without crossflow

Figure 3(a) shows vorticity contours for two vortex rings generated by stroke ratios of 6 and 2 respectively. In the case of higher stroke ratio, a vortex ring followed by a trailing column of fluid is generated (figure 3a). The time evolution of total circulation of the flow field, and vortex ring circulation are shown in figure 3(b) for $L/D = 6$. Vortex ring circulation is estimated only after it clearly pinches off from the trailing jet. The formation number defined by Gharib *et al.* (1998), is 'the formation time when the total circulation imparted by the discharging flow is equal to the circulation of the pinched off vortex ring'. Their study showed the existence of a limiting value for the stroke ratio (L/D), above which the vortex ring does not absorb all the vorticity of the discharged fluid. They conclude that there is a maximum value of circulation that a vortex ring can acquire as the stroke ratio increases. This maximum is reached at a piston stroke ratio of $L/D \approx 4$. In the simulation, the formation number is found to be approximately 3.6 from the circulation plot in figure 3(b). Also shown are results from Gharib et al's experiments (1998). Good agreement with experiment is observed. So, the formation number is the transition stroke ratio which separates the two regime of ring structure. If the stroke ratio is higher than the formation number, the excess circulation accumulates in the

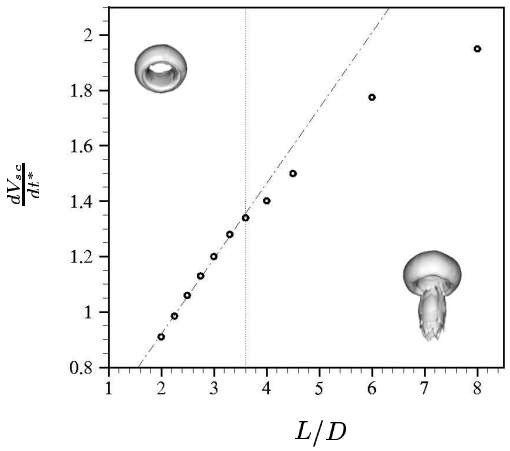

Figure 5. The rate of scalar volume after formation is plotted against the stroke ratio. The dotted line separates the two regime of flow - stroke ratio less than formation number and higher than formation number. The corresponding flow structures (iso–surface of vorticity) are also shown for the two regimes.

jet like trailing column as shown in figure 3(a). For stroke ratio less than formation number, a single vortex ring is generated leaving behind a quiescent flow.

Evolution of passive scalar is studied to investigate the mixing and entrainment characteristics of vortex rings without crossflow and the effect of stroke ratio on these characteristics. The scalar concentration of fluid emerging out from the nozzle and crossflow fluid are 1.0 and 0.0 respectively. Figures 5(a) and 5(b) show instantaneous scalar contours after formation, for vortex rings with stroke ratio 2 and 6 respectively. The scalar profiles along a line passing through the core centers reveal that the scalar mixing inside the vortex ring is similar for both of the cases. At the boundary of the ring, the scalar diffuses because of the gradient between the ring fluid and ambient fluid. This diffused scalar is deposited by the ring in its wake. The scalar in the trailing jet also diffuses into the ambient fluid. In the ring core, the boundary layer fluid from the nozzle is stretched, and mixed with entrained ambient fluid. During the formation of vortex ring, the ambient fluid near the nozzle exit is radially entrained into the vortex ring. As the ring forms, a region of very low pressure is created outside the nozzle, at the center of the vortex core. The resulting pressure gradient is directed towards the vortex center, and causes ambient fluid to be entrained. Figure 4(a) shows the horizontal cross section of the emerging shear layer for the case of $L/D = 2$ at a height of at $y/D = 0.1$ at $t^*= 1.008$. In–plane velocity vectors are shown along with scalar contours. The velocity vectors show the motion of the ambient fluid toward the edge of the fluid emanating from the nozzle–exit. These results show that ambient fluid is radially entrained into the vortex ring, from the near field of the nozzle, during the formation phase. For the case of $L/D = 6$, the leading vortex ring entrains the ambient fluid during its formation. However, the trailing jet does not entrain ambient fluid similar to ring. Figure 4(b) shows the horizontal cross–section of the trailing jet for $L/D = 6$ at $y/D = 0.6$ at $t^*= 5.04$. The absence of appreciable radial entrainment is apparent; the trailing column is mostly surrounded by stationary fluid. We seek to find which structure is better in terms of mixing. In other words, for a given amount of fluid, what should be the stroke ratio for most effective mixing?

Total volume of scalar carrying fluid (V_{sc}) is computed for different stroke ratios. V_{sc} is found to vary linearly with time after the inflow stops. Figure 5(c) plots the rate of change of V_{sc} after formation ($t^* > L/D$) for different stroke ratios. The rate is computed from the slope of the linear V_{sc} curve with time. Note that the rate increases linearly with stroke ratio until the stroke ratio equals the formation number. For stroke ratio grater than the formation number, the rate falls below the linear curve. The deviation increases with

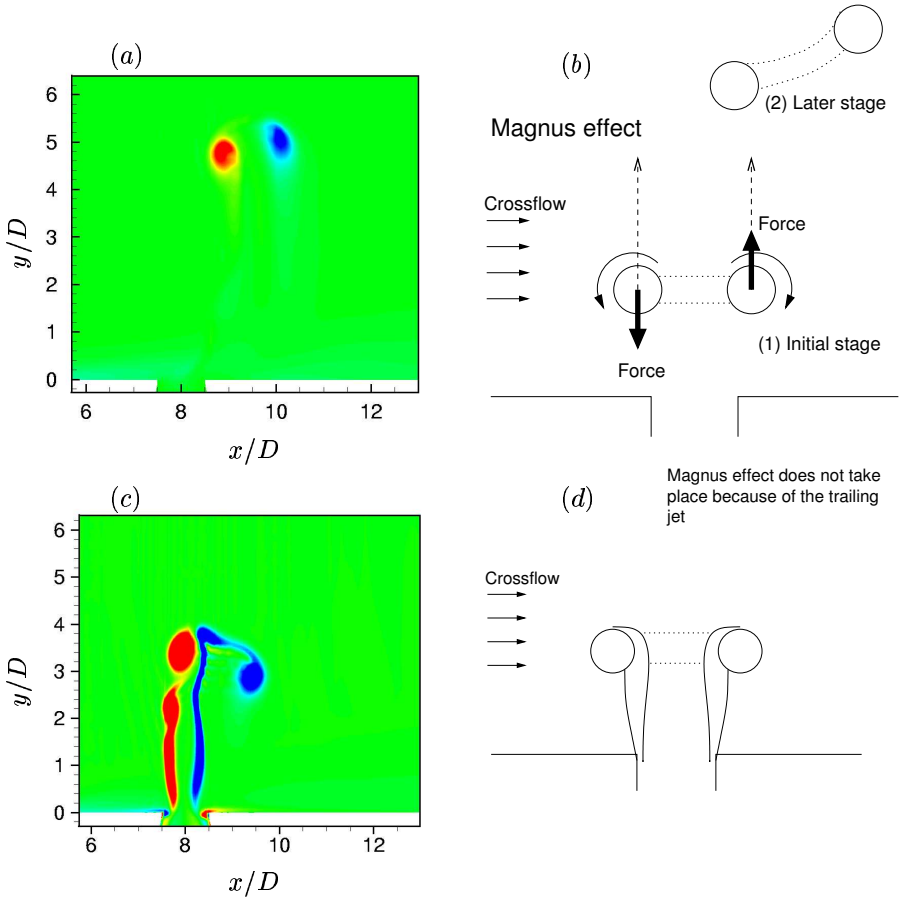

Figure 6. Vortex ring in crossflow. Vorticity contours in the symmetry plane ($z = 0$) for L/D = (a) 2 & (c) 6. Schematics to explain vortex ring tilting using Magnus effect - (b) & (d).

increasing stroke ratio, and may be explained as follows. Stroke ratios smaller than formation number yield vortex ring without trailing column. The size of the vortex ring increases with increasing stroke ratio, until the formation number is reached, since all the nozzle fluid goes into the vortex ring. The largest possible vortex ring is therefore produced at the formation number. This increase in ring size results in increased rate of mixing. As the stroke ratio increases beyond the formation number, the flow field consists of the leading vortex ring and trailing column. Increasing the stroke ratio does not change the leading vortex ring; it only increases the length of the trailing column. The overall entrainment may be thought to be a combination of entrainment by the leading vortex ring, and entrainment by the trailing column. The relative contribution of the leading vortex ring to the overall entrainment therefore decreases as the stroke ratio increases. Again, the trailing column does not entrain fluid as effectively as the vortex ring. This results in an overall decrease of entrainment as the stroke ratio increases beyond the formation number. So, the optimal stroke ratio is the formation number for vortex rings without crossflow.

In the case of pulsed jet with square wave excitation, each cycle or time period produces a vortex ring. The stroke ratio of these rings can be obtained from the Strouhal number (St) and duty cycle (α) of pulsation as shown in §2. Vortex ring with maximum circulation (i.e. maximum induced momentum) is produced at the stroke ratio of formation number or beyond. These rings will penetrate deeper than those created by stroke ratio less than formation number. In terms of mixing and entrainment, as discussed earlier, trailing

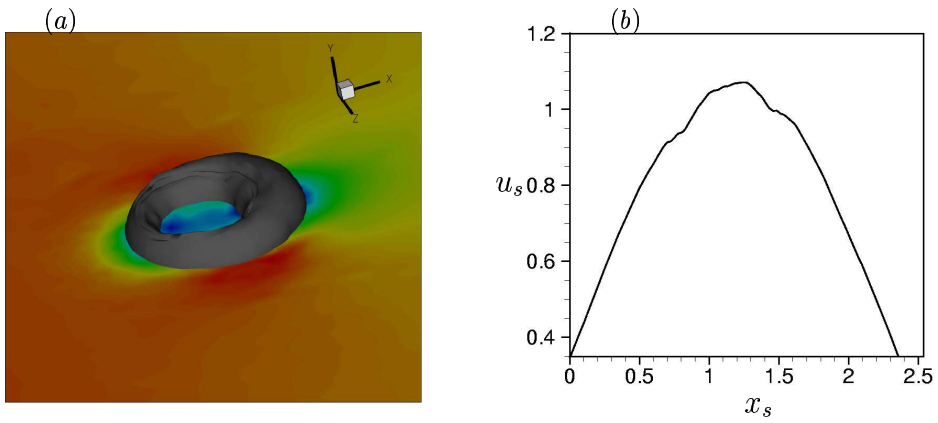

Figure 7. (a) Vortex ring structure for L/D of 2 along with contours of in–plane velocity magnitude (b) The in–plane velocity magnitude plotted on the curve which encompasses the circumference of the ring from upstream side to downstream side on the plane of the ring.

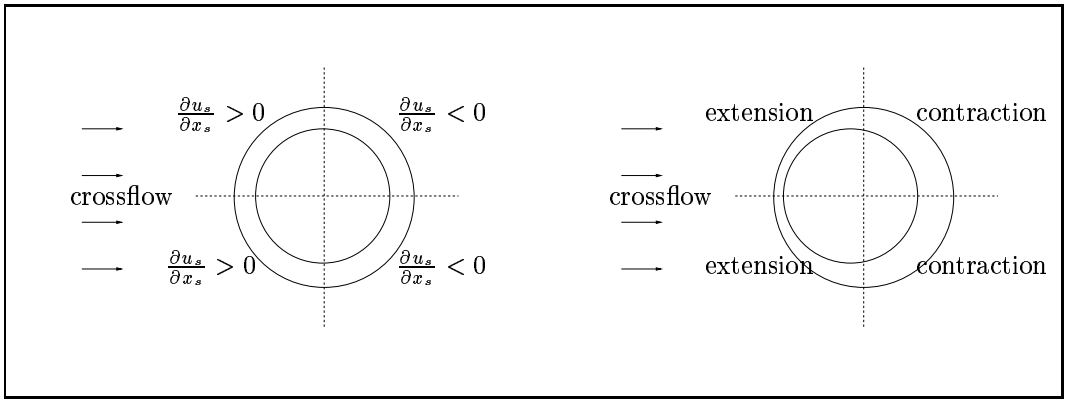

Figure 8. A schematic to show the velocity gradients along the ring, set up by the crossflow and the deformation of the ring because of the velocity gradient.

column effectively reduces the overall volume rate of mixing. These results suggest that the frequency and duty cycle should be such that the stroke ratio is near the formation number or at least not larger than formation number to avoid trailing column. However, the results for the case of vortex ring in crossflow show that the trailing column plays the most significant role in mixing and entrainment. The following section examines the effect of crossflow on vortex rings.

B. Vortex ring in crossflow

1. Vortex ring dynamics

Simulations of a vortex ring in crossflow show that the ring tilts and deforms. Figure 6(a) and 6(c) show vorticity contours of vortex rings in crossflow with stroke ratio 2 and 6 respectively. The velocity ratio is 3 in both cases. The vortex ring in 6(a) tilts such that its induced velocity opposes the crossflow. Whereas, the vortex ring with stroke ratio 6 tilts in the opposite direction; here leading vortex ring tilts in the direction of the crossflow. As a result, this ring's induced velocity has a component along the direction of the crossflow.

The Magnus effect may be used to provide a simple explanation for these tilting behavior. In the case

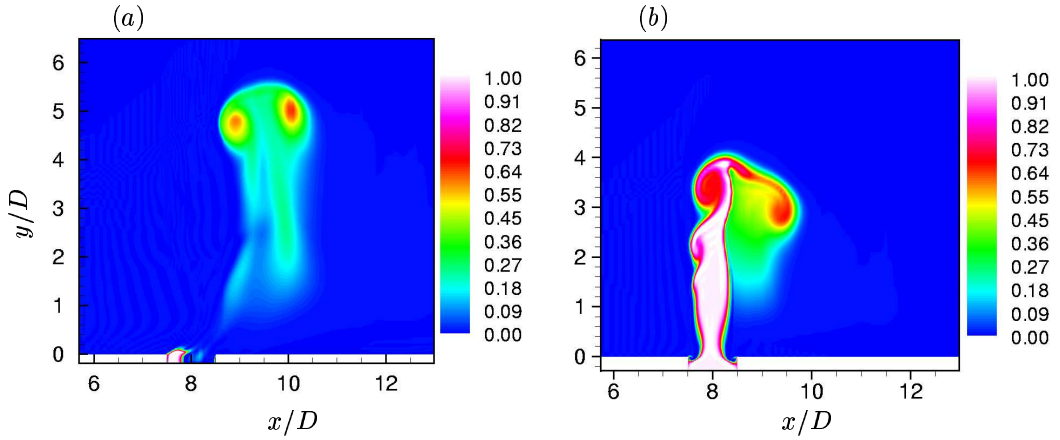

Figure 9. Instantaneous scalar contours on the symmetry plane for vortex ring in crossflow with r=3 and L/D of (a) 2 & (b) 6. Note asymmetry in the scalar concentration in the case of small stroke ratio. Also Note the enhanced downstream mixing for the case of large stroke ratio.

of single ring without trailing column, the crossflow sees the upstream side of the ring as an anticlockwise rotating cylinder with fixed circulation. So, the crossflow exerts a downward Magnus force on the upstream side of the ring as shown in a schematic in figure 6(b). The downstream side of the ring similarly experiences an upward Magnus force. As a result, the ring tilts to oppose the crossflow. In the second case for large stroke ratio, the crossflow sees the incoming fluid from the nozzle as a starting continuous jet. The trailing column acts as an obstacle to the crossflow. As a result, the Magnus effect does not take place as shown in figure 6(d). The crossflow bends the leading vortex ring and the trailing column along the direction of the crossflow.

The '*equivalent formation number*' for vortex rings in crossflow can be derived from this tilting behavior. As noted earlier the tilting behaviors of single ring and ring with trailing column are opposite in nature. The equivalent formation number can be defined as the transition stroke ratio at which the direction of tilting changes. At first, it is intuitive to conclude that equivalent formation number is same as the formation number of vortex rings without any crossflow. But the simulation results suggest that the equivalent formation number depends on the velocity ratio r. In fact, it will be shown that the crossflow actually decreases the formation number.

The vortex ring also deforms in the presence of crossflow. The downstream side of the ring becomes thicker than the upstream side. Figure 7(a) shows the ring along with the contours of in–plane velocity magnitude on the plane of the ring. The deformation of the ring can be explained by vortex tube extension/contraction. The vorticity transport equation is:

$$\frac{\partial \Omega_i}{\partial t} + u_j \frac{\partial \Omega_i}{\partial x_j} = \Omega_j \frac{\partial u_i}{\partial x_j} + \nu \frac{\partial^2 \Omega_i}{\partial x_j x_j}$$

Here, the term $\Omega_j \frac{\partial u_i}{\partial x_j}$ accounts for the vortex stretching and tilting. The extension or contraction of a vortex element depends on the velocity gradient along the direction of vorticity. If the velocity gradient is positive along a vortex element, then the vortex element will be stretched and vorticity will increase. As a result, the vortex tube becomes thin in size. The vortex tube becomes thicker in the case of contraction due to negative velocity gradient. The velocity magnitude on the vortex ring plane is shown in figure 7(a). Figure 7(b) plots the in–plane velocity magnitude along a curve which encompasses the circumference of the ring from upstream side to downstream side. The velocity field around the ring is such that it sets up a positive velocity gradient along the ring in the upstream side and a negative velocity gradient along the ring in the downstream side. The velocity gradient experienced by the ring and the deformation is shown in a schematic

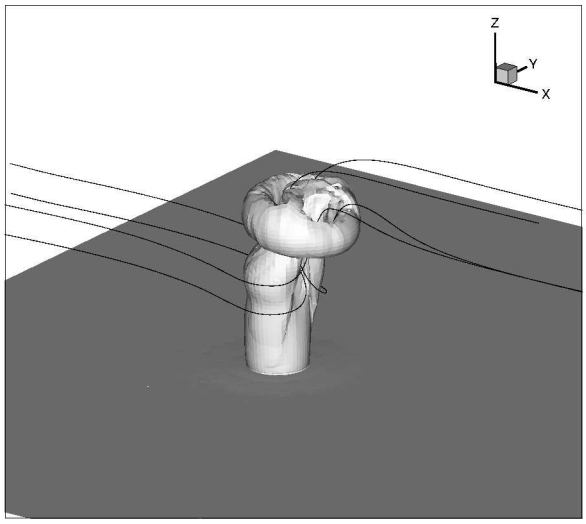

Figure 10. Iso–surfaces of vorticity along with some 3D streamlines for the case of $L/D = 6$ and $r = 3$. The stream lines show the downstream entrainment of the crossflow fluid.

in figure 8. The upstream side of the ring experiences a positive velocity gradient and stretches as a result. The downstream side exhibits the opposite behavior.

2. Mixing characteristics

Transport of passive scalar is used to study the mixing and entrainment characteristics of the vortex ring in crossflow. Figure 9 shows the instantaneous scalar contours for two different vortex rings in crossflow. In both the cases the the velocity ratio is 3. The stroke ratios of the vortex rings are 2 and 6 in figure 9(a) and figure 9(b) respectively. Distinctly different mixing and entrainment behavior can be observed in both rings. In the first case, a single tight ring is produced. The scalar contours are similar to the case without crossflow except there is an asymmetry in the ring. The scalar contours show the upstream side of the ring is more mixed than the downstream side of the ring. However, for the case of large stroke ratio, the scalar contours in figure 9 clearly shows that mixing in the downstream side is enhanced significantly. In the first case the asymmetry in scalar mixing can be attributed to the deformation of the ring as explained in the earlier section. The mixing characteristics for the two regime of stroke ratio are totally opposite in nature. The behavior of the second case (i.e. for large stroke ratios) can be explained as follows in the next paragraph.

For large stroke ratios, the vortex ring along with trailing column appear as a starting jet in crossflow. As noted by Muppidi & Mahesh (2006), when a jet encounters a crossflow, a high pressure gradient is created toward the jet on the downstream side. This pressure gradient drives the flow toward the jet and causes the jet to entrain lot more fluid on the downstream side rather than upstream side. Similarly, in the case of vortex ring with trailing column, the trailing column acts as an obstacle to the crossflow fluid. The crossflow fluid goes around the trailing column before the crossflow momentum succeeds to bend the starting jet. A similar downstream pressure gradient is created toward the ring and trailing column as in jet in crossflow. Figure 10 explains this downstream entrainment. Iso–surfaces of vorticity along with some $3D$ streamlines of the flow field are shown in figure 10 for the case of $L/D = 6$ and $r = 3$. The iso–surfaces show the structures of the ring along with the trailing column. It is interesting to observe the streamlines in this figure 10. The streamlines clearly show that the crossflow fluid goes around the trailing column and is entrained from the downstream side in to the trailing column and vortex ring. This entrainment is due to the downstream pressure gradient as stated earlier. However, in this particular case there is also a vortex ring above the

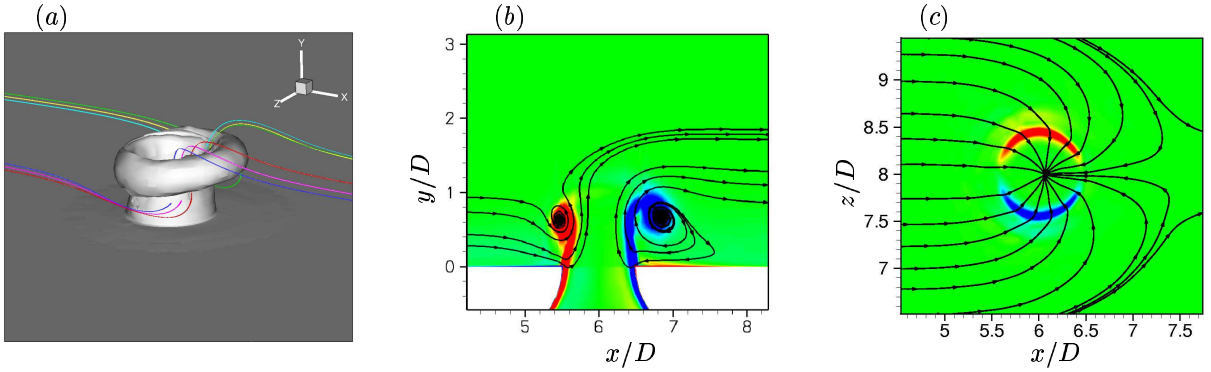

Figure 11. Results for the case of $L/D = 2$ and $r = 1.5$ during the formation phase of the ring. (a) Iso–surfaces of vorticity along with some 3D streamlines. (b) Vorticity (Ω_z) contours along with streamlines on the symmetry plane $z = 0$. (c) Contours of x-component of vorticity (Ω_x), along with in–plane streamlines on a horizontal plane ($y/D = 0.25$). Note the crossflow entrainment along with the entrainment of shear layer fluid during the formation of the ring.

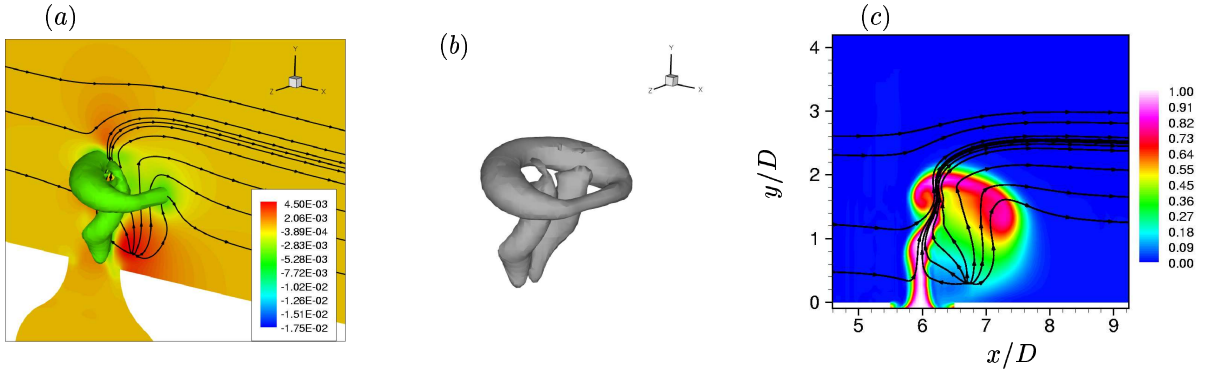

Figure 12. Results for the case of $L/D = 3$ and $r = 1.5$ after the formation phase of the ring. (a) The pressure contours in the symmetry plane ($z = 0$) along with some in–plane streamlines. The iso–surface of pressure is also plotted to show the ring and trailing column structure. (b) The ring and trailing column structure. (c) Instantaneous scalar contours along with some streamlines in the plane of symmetry.

trailing column, and the ring is tilted toward the crossflow. Again, the vortex ring core is a region a very low pressure. This further enhances the downstream pressure gradient which in turn increases the downstream entrainment of the ambient fluid. So, the overall entrainment increases significantly due to the existence of a trailing column. Unlike the case of vortex ring in stationary fluid, the trailing column plays a very significant role in mixing and entrainment, in the presence of crossflow. Also it is important to note in figure 10 that the trailing column has started to deform in shape on the downstream side. This deformation causes the downstream pressure gradient.

§1 introduced the notion of equivalent formation number in crossflow. Figure 11(b) shows the out of plane vorticity contours along with some streamlines in the plane of symmetry during the formation of the ring of $L/D = 2$. The vortex ring formation is contributed by the fluid from the shear layer along with the entrained crossflow. Figure 11(c) shows the horizontal cross section of the flow field at a height of $y/D = 0.25$. This figure shows cross section of the shear layer in terms of the contours of x component of vorticity and some in–plane streamlines. During the formation phase of the ring itself, the crossflow causes the increase in entrainment of ambient fluid. Without the crossflow, the fluid near the nozzle exit is radially entrained into the ring. In the case of crossflow, this entrainment is enhanced in the upstream side as the

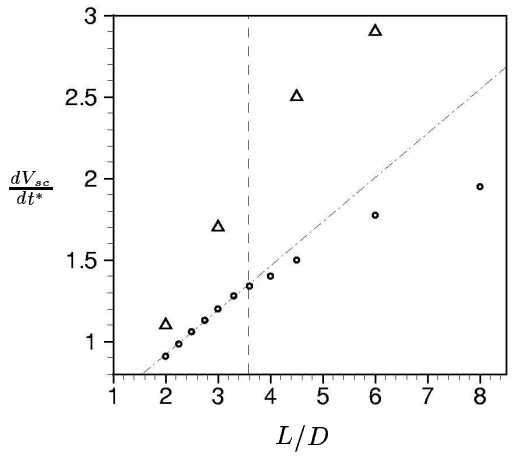

Figure 13. The rate of change of scalar volume after formation is plotted against the stroke ratio for the velocity ratio $r = 1.5$: $-\triangle-$. The results for the vortex rings in the absence of crossflow are also shown: $-\circ-$.

crossflow direction favors this entrainment. In the downstream side also, the crossflow fluid is entrained into the ring. Figure 11(a) helps to visualize the flow field. The shear layer along with the forming vortex ring structure and the entrainment of crossflow fluid is evident. Now, the ring formation is mostly contributed by the entrainment of the shear layer fluid which emerges from the nozzle. As we increase the stroke ratio (in the regime less than formation number), it is possible to end up with a vortex ring and a trailing column. In such a case, the entrainment of the crossflow fluid does not allow all of the shear layer from the nozzle to be entrained by the ring. Hence, the vortex ring leaves a trailing column behind it. Of course, this depends on the velocity ratio. For low velocity ratio, the scenario is more likely to happen for stroke ratios even less than formation number. It can be thought of as a competition between the entrainment of crossflow fluid and shear layer fluid from the nozzle into the ring.

Figure 12(a) shows pressure contours along with some streamlines in the symmetry plane for vortex ring with $L/D = 3$ and $r = 1.5$. The iso-surface of pressure is also plotted to show the vortical structure. Note that a strong trailing column exist in this case. Figure 12(b) plots only the iso-surfaces to show the vortical structures separately. The vortex ring is tilted toward the direction of the crossflow. The downstream side of the ring becomes considerably thin as it mixes with the crossflow fluid. The trailing column is highly deformed which causes a very high pressure gradient toward the ring and the trailing column itself in the downstream side. The downstream pressure gradient is evident from the pressure contours shown in figure 12(a). The streamlines show the downstream entrainment of crossflow fluid because of this pressure gradient. These results suggest that even at stroke ratio of 3, a single vortex ring is not possible. Instead a strong trailing column exists thus lowering the formation number. So the equivalent formation number is certainly less than 3 for this particular case of velocity ratio 1.5. Figure 12(c) shows the scalar contours along with some in–plane streamlines in the symmetry plane for the case of $L/D = 3$ and $r = 1.5$. The ring is tilted toward the crossflow direction. The downstream enhancement of mixing and entrainment due to the existence of trailing column is evident from the contours and streamlines.

In order to quantify the effect of crossflow on overall scalar mixing, the rate of total volume of scalar after formation is computed. The procedure is similar to the case of vortex ring without crossflow. Figure 13 shows the rate with different stroke ratios for velocity ratio of 1.5 along with the results for rings without crossflow. The figure suggests that the crossflow enhances the mixing in each of the cases. But the enhancement is much higher for larger stroke ratios. For stroke ratio of 2, the rate of volume change increases only about 20%. The increase is about 41% for stroke ratio of 3 and about 66% for both the stroke ratios - 4.5 and 6.

It is shown earlier that the equivalent formation number in the case of $r = 1.5$ is less than 3. The existence of the trailing column in each the stroke ratios except 2, increases the mixing and entrainment. And these results also suggest that the trailing column is desirable for increased mixing in vortex rings.

IV. Conclusion

Direct Numerical Simulations are performed to study vortex rings in the presence and absence of crossflow. In the absence of crossflow, passive scalar mixing are studied for the two different flow structures - vortex ring and vortex ring with trailing column. Simulations show that the trailing column does not entrain as effectively as vortex rings. The rate of volume change of scalar carrying fluid after formation was examined, and seen to vary linearly with stroke ratio until the formation number is reached. As the stroke ratio increases beyond the formation number, the rate increasingly deviates away from the linear curve. This suggests that generation of trailing column is best avoided, if the objective is to entrain and mix as much as ambient fluid as possible. So, the optimal stroke ratio is shown to be at the formation number in the absence of crossflow.

The crossflow tilts and deforms the vortex rings. The single vortex ring tilts towards the opposite direction of the crossflow such that its induced velocity opposes the crossflow. The Magnus effect is used to provide a simple explanation of this tilting. The ring also deforms because of the vortex stretching due to velocity gradient imposed by the crossflow. The downstream side becomes more thick than the upstream side. On the other hand, vortex ring with trailing column is tilted along the direction of the crossflow. A high pressure gradient is created on the downstream side due to the deformation of the trailing column. The downstream portion of the tilted–leading–ring further enhances this pressure gradient which increases the downstream entrainment significantly which in turn improves the overall mixing and entrainment by a significant amount. So, in the presence of crossflow, the vortex ring along with the trailing column is shown to be most effective in mixing and entrainment unlike the case for vortex rings without crossflow.

During the formation of the vortex rings, the crossflow fluid is entrained along with the shear layer fluid from the nozzle into the vortex core. Although the formation of vortex rings is mostly contributed by the shear layer fluid from the nozzle, the entrainment of the crossflow fluid depending on the velocity ratio does not allow all of the shear layer fluid to be entrained in to the ring even at stroke ratios less than formation number. Therefore, the crossflow reduces the stroke ratio after which the trailing columns are formed. It is shown that a strong trailing column is formed and the ring is tilted toward the direction of the crossflow at $L/D = 3$ and $r = 1.5$. The rate of volume change of scalar carrying fluid after formation was also examined in the presence of crossflow. The crossflow increases the rate, but the increment is much higher in the case of higher stroke ratio as a result of the formation of trailing column which results in enhanced entrainment of the crossflow fluid on the downstream side.

V. Acknowledgments

This work was supported by the National Science Foundation under grant CTS–0133837. Computer time was provided by the National Center for Supercomputing Applications (NCSA), Minnesota Supercomputing Institute (MSI) and the San Diego Supercomputer Center (SDSC). We thank Dr. Suman Muppidi for helpful discussions.

References

[1]Blossey, P., Narayanan, S. & Bewley, T.R., 2001 Dynamics and control of a jet in crossflow: direct numerical simulation and experiments. *Proc. IUTAM Symp. Turbulent Mixing Combustion*, ed. A. Pollard & S. Candel, Kluwer Academic, Dordrecht, pp. 45–56.

[2]Eroglu, A. & Briedenthal, R.E., 2001 Structure, penetration and mixing of pulsed jets in crossflow. *AIAA J.* **39(3):** 417–423.

[3]Gharib, M., Rambod, E. & Shariff, K., 1998 A universal time scale for vortex ring formation. *J. Fluid Mech.* **360:** 121–140.

[4]Johari, H., 2006 Scaling of fully pulsed jets in crossflow. *AIAA J.* **44(11):** 2719-2725.

[5]Karagozian, A.R., Cortelezi, L. & Soldati, A., 2003 Manipulation and control of jets in crossflow, CISM Courses and Lectures No. 439, International Center for Mechanical Sciences, Springer Wien, New York.

[6]Mahesh, K., Constantinescu, G. & Moin, P., 2004 A numerical method for large–eddy simulation in complex geometries. *J. Comput. Phys.* **197:** 215–240.

[7]Muppidi, S., 2006 Direct Numerical Simulations and Modeling of jets in crossflow. *PhD Thesis*, University of Minnesota.

[8]Muppidi, S. & Mahesh, K., 2006 Passive scalar mixing in jets in crossflow. *AIAA* Paper 2006-1098 .

[9]M'Closkey, R.T., King, J.M., Cortelezzi, L. & Karagozian, A.R., 2002 The actively controlled jet in crossflow. *J. Fluid Mech.*, **452:** 325–335.

[10]Rosenfeld, M., Rambod, E. & Gharib, M., 1998 Circulation and formation number of laminar vortex rings. *J. Fluid Mech.* **376:** 297–318.

[11]Shapiro, S.R., King, J.M., Karagozian, A.R. & M'Closkey, R.T., 2003 Optimization of controlled jets in crossflow. *AIAA Paper* 2003–634.